ACS APPLIED ENERGY MATERIALS
Cite This: ACS Appl. Energy Mater. 2019, 2, 2579−2584
Article
www.acsaem.org

Favoring the Reactivity of TiO_2 Films with Ideal Arrangement of Anatase and Rutile Crystallites

Iuri S. Brandt,*[,†] Daniel G. Stroppa,[‡] Paulo N. Lisboa-Filho,[§] José H. D. da Silva,[§] and André A. Pasa[†]

[†]Laboratório de Filmes Finos e Superfícies, Universidade Federal de Santa Catarina, Florianópolis 88040-900, Brazil
[‡]INL − International Iberian Nanotechnology Laboratory, Av. Mestre José Veiga, 4715-330 Braga, Portugal
[§]Faculdade de Ciências, UNESP - Universidade Estadual Paulista, Bauru, SP 17033-360, Brazil

Supporting Information

ABSTRACT: It is shown that there are deposition conditions in reactive sputtering of TiO_2 in which the anatase and rutile crystals can coherently arrange in a convenient way that predominantly exposes the anatase facets, a configuration that is expected to favor the photocatalytic activity of the films. The latter process plays at present an important role in environmental conservation related to energy generation and water cleaning. Therefore, our results present an experimental path for obtaining highly photoreactive TiO_2 films.

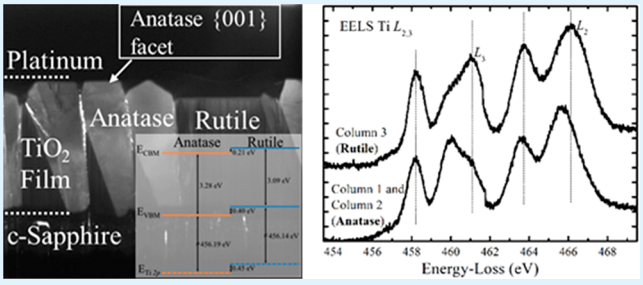

KEYWORDS: *anatase, rutile, photocatalysis, coherent growth, reactive sputtering*

1. INTRODUCTION

At present, photocatalytic processes play a critical role in environmental conservation related to energy generation and water cleaning. Within this context, because of its desired characteristics for photocatalytic applications, TiO_2 has been intensively investigated, and several findings have brought the understanding of the properties of TiO_2 phases to a new level.[1−3] For anatase TiO_2, several results indicate that its {001} facets are the most efficient for photocatalysis.[4−9] However, few works report experimental routes for obtaining anatase crystallites with a high percentage of {001} facets,[4−8] since rutile is the most stable TiO_2 phase against temperature[10] and also because near-equilibrium anatase growth tends to hide the highly reactive {001} facets.[11] These difficulties bring additional challenges for improving the number of {001} facets of anatase TiO_2 crystals and reveal the importance for controlling the growth kinetics and the role of interfaces during TiO_2 film formation.

Furthermore, in different reports, it was observed that TiO_2 samples composed by both polymorphs anatase and rutile present enhanced photocatalytic activity over the single-phase one.[12−17] The key factor for this synergistic effect is the favorable band alignment between anatase and rutile phases that allows spatial charge separation avoiding the electron−hole pair recombination.[18,19]

Therefore, anatase−rutile TiO_2 samples with anatase {001} facets are desirable for highly efficient photocatalysis. In this sense, here we demonstrate that the growth of TiO_2 films onto *c*-plane sapphire is an efficient combination to promote a peculiar distribution of anatase and rutile crystallites, in which the anatase {001} surface is obtained. Moreover, a type II band alignment between anatase and rutile crystals is likely to occur, which is a configuration that favors the photocatalytic activity of the films.[18,19]

2. EXPERIMENTAL METHODS

The films were prepared in a radio frequency reactive magnetron system using a pure Ti target (5 N purity) and a mixture of Ar and O_2 gases (flow rates: 40.0 sccm/5.0 sccm Ar/O_2, 6 N purity both). Sapphire *c*-plane was used as substrates. The target diameter was 75 mm, and the target to substrate distance was 70 mm. A deposition power of 180 W, with reflected fraction below 2 W, and measured RMS bias of 138 V were kept constant with a regulated source and RF matching box (Advanced Energy RFX 600). A relatively high substrate temperature (550 °C) and relatively low total pressure 2.5 × 10^{-3} Torr were used to produce film crystallization and significant rutile fraction.[20] The discharge parameters were stable within 4% during all depositions. The main variations were observed in the total pressure, being the other variations of the order of 1%. The method has the potential to be used for production in large areas, provided the power density of the discharge is kept by suitable power supply and target dimensions. Before depositions, a cleaning procedure was performed in the target. This consists of sputtering the target in pure Ar, 120 W, for 3 min, and then in a stabilization of the Ar/O_2 mixture (40.0 sccm/5.0 sccm) and plasma parameters for more 3 min before the start of depositions.

Cross-section samples of the grown films were prepared using a focused ion beam (FEI Helios NanoLab 450S). A 2 μm protective Pt layer was deposited over the thin film to reduce sample damage and ions' implantation on the subsequent sample preparation, and then 30 kV Ga^+ ions were used to cut off a thin lamella containing the TiO_2−

Received: December 18, 2018
Accepted: March 20, 2019
Published: March 20, 2019

DOI: 10.1021/acsaem.8b02171
ACS Appl. Energy Mater. 2019, 2, 2579−2584

sapphire interface. The lamella final thinning/polishing was carried with 2 kV Ga^+ ions to ensure a minimized amorphous layer.

High-resolution transmission electron microscopy (HRTEM) and electron energy loss spectroscopy (EELS) measurements were performed on a FEI Titan3 Themis 300 operating at 80 kV. EELS experiments were performed in scanning transmission electron microscopy (STEM) mode with a monochromatic beam with energy spread lower than 0.13 eV. Spectra were collected using a Gatan Enfinium ER 977 spectrometer with a 0.01 eV/pixel dispersion to retain the high energy resolution from the monochromated source. Low-loss spectra were collected with 0.2 s frame time and 20 s total time, and core-loss spectra at Ti−K and O−K edge energy were collected with 5 s frame time and 350 s total time.

The film morphology was investigated by scanning electron microscopy (SEM) with a Helios 450S (FEI). The structural characterization was performed by X-ray diffraction (XRD) using a PANalytical X'PERT X-ray system with Cu $K\alpha_1$ radiation. The pole figures were performed by electing a diffraction angle, 2θ, with the tilt angle, χ, varying from 0 to 90° and the azimuthal angle, ϕ, varying from 0 to 360°, for each value of χ.

Details of further structural characterizations may be found in the Supporting Information.

3. RESULTS AND DISCUSSION

A plan-view SEM image of a thick (2.5 μm) TiO_2 film deposited onto *c*-plane sapphire is shown in Figure 1a. It is possible to observe that the film surface is composed of parallelepiped, pyramidal grains, and flat regions between them. In the inset of Figure 1a the three morphologies are respectively numbered as 1, 2, and 3. A cross-section STEM image is presented in Figure 1b. A columnar structure is observed, where higher and brighter columns are associated with two different shapes on the top: trapezoidal (column 1) and triangular (column 2). The darker ones are flat on the top (column 3). The brighter columns grow by increasing width at the expense of neighboring ones (darker columns) which assume a prism-like shape. These three shapes match to the parallelepiped, pyramidal grains, and flat region observed from above in the SEM image. Figure 1c displays a high-resolution TEM image of the interface between structures 2 and 3, and in that interface no amorphous phase is observed.

To identify the nature of the observed regions seen in Figure 1, EELS measurements were carried out. The Ti $L_{2,3}$ main edges associated with columns marked as 1, 2 and 3, in Figure 1 are shown in Figure 2a. EELS Ti $L_{2,3}$ results from columns 1 and 2 showed practically identical spectra and are similar to spectrum obtained in column 3. The L_3 and L_2 edges are separated by ∼5 eV due to the 2p core−hole spin−orbit coupling. The phase identification relies on the details of the spectra. The oxygen atoms, surrounding each titanium atom, create a strong crystal-field splitting that subdivides both Ti L_3 and Ti L_2 edges. In columns 1 and 2 the splitting of the L_2 edges is 2 eV, while in column 3 the splitting is 2.4 eV. These are the values expected for anatase and rutile phases, respectively.[21] The L_3 edge of columns 1 and 2 presents a more prominent low-energy component, which is a feature attributed to anatase phase.[21] Meanwhile, the L_3 edge of column 3 shows a stronger component at the higher energy side, characteristic of a rutile crystal.[21]

The EELS O-K edges are shown in Figure 2b. The main peaks, marked with vertical dotted lines, display splittings of 2.5 eV (column 1) and 2.7 eV (column 3). These splittings are expected[21] for anatase and rutile, respectively. Additionally, there exist differences between column 1 and 3 O-K spectra in the broad peaks ∼8−15 eV far from the main peak at 532.4 eV.

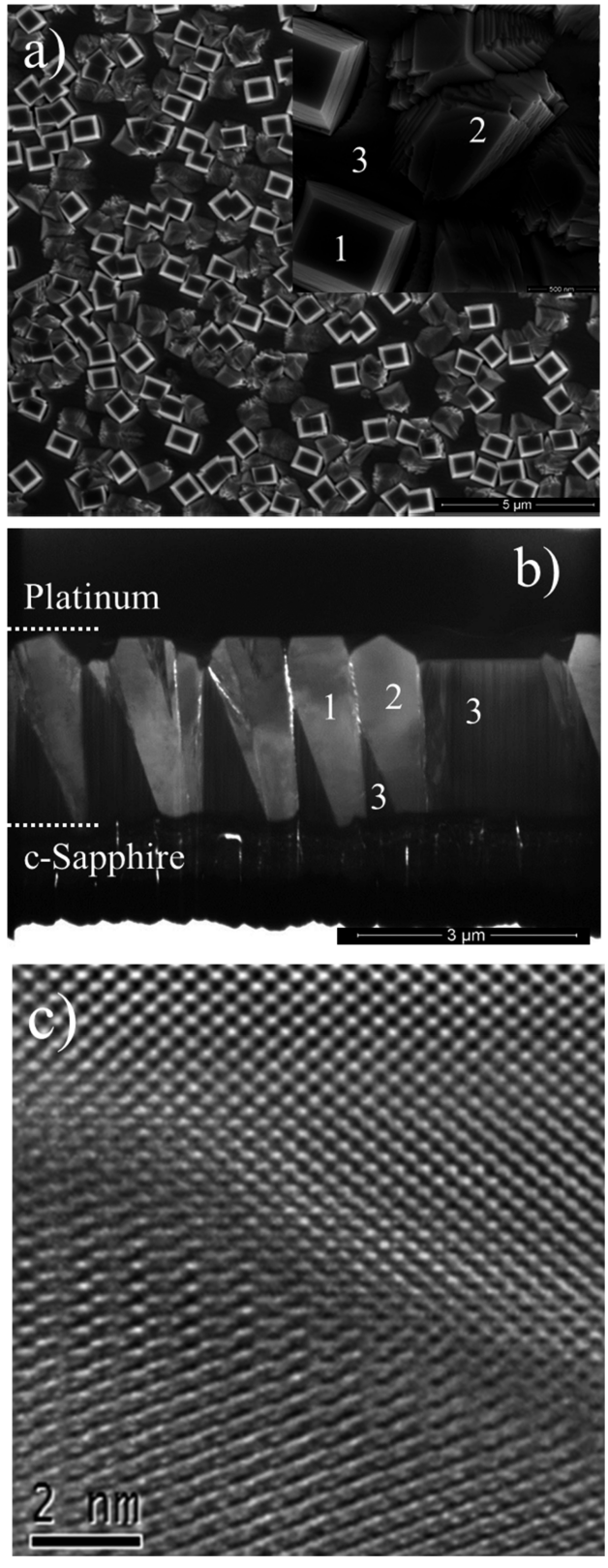

Figure 1. (a) Scanning electron microscopy of a TiO_2 film grown on *c*-sapphire substrate and (b) transmission electron microscopy bright-field image of the cross section of the same film. In the transmission image the columns are numbered accordingly. The predominantly columnar morphology of the internal parts of the TiO_2 film is visible. Using the EELS results presented in the sequence, the underneath triangular-shaped smaller grains near the substrate interface were identified to have the same phase as the columns labeled 3. The inset

DOI: 10.1021/acsaem.8b02171
ACS Appl. Energy Mater. 2019, 2, 2579−2584

Figure 1. continued

in (a) shows, with higher magnification, the surface morphology formed by cubic and pyramidal grains and a flat region, numbered as 1, 2, and 3, respectively. (c) High-resolution transmission electron microscopy of interface between columns 2 (anatase) and 3 (rutile) shown on the rutile [001] axis zone.

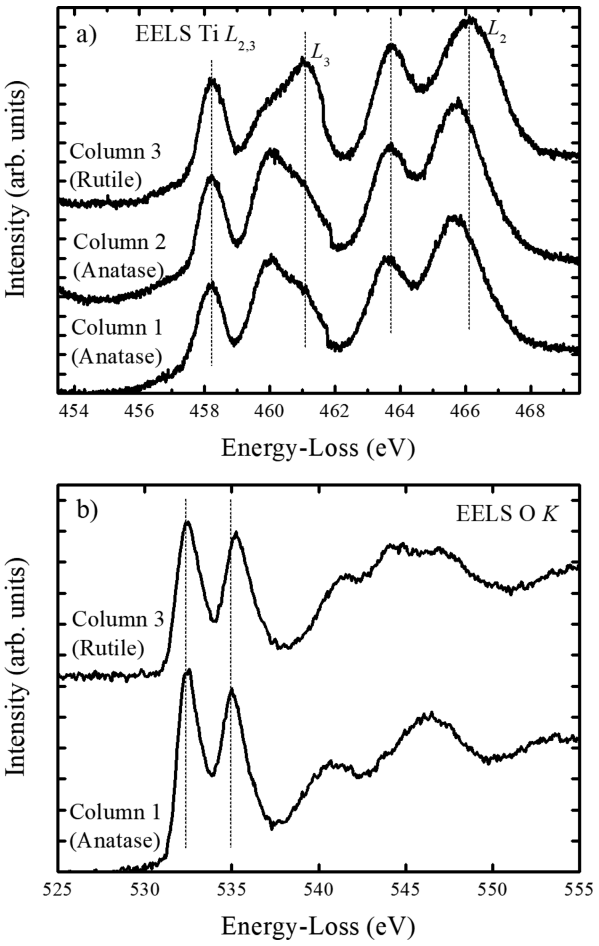

Figure 2. EELS spectra associated with the different regions shown in Figure 1. (a) Ti $L_{2,3}$ main edges measured on regions 1 and 2, attributed to anatase, and measured on region 3, attributed to rutile. (b) EELS O-K edges measured on region 1, related to anatase, and measured on region 3, attributed to rutile. From the EELS O-K edge it is observed a peak splitting of 2.5 eV (column 1) and 2.7 eV (column 3), characteristics of anatase and rutile phases, respectively. The vertical dotted lines are traced to serve as guides to the peak splittings.

Such features are in accordance with EELS and XAS spectra found in the literature for anatase and rutile TiO_2 phases.[21]

EELS low-loss spectra of columns 1 and 3 are presented in Figure 3. The peak near 14 eV that shows up clearly in the curve of column 3 can be attributed to rutile,[22] in agreement with the previous analysis. The low-intensity region, from ∼3 to 8 eV, corresponds to electronic transitions from the valence band edge (O 2p orbitals) to the bottom of the conduction band (Ti 3d orbitals). The fittings for an indirect band gap[23] are depicted in the inset of Figure 3 by continuous lines. This procedure yields an E_g of 3.09 and 3.28 eV for rutile (column 3) and anatase (column 1), respectively. Such values agree with the ones found in the literature for rutile[24] and anatase.[25]

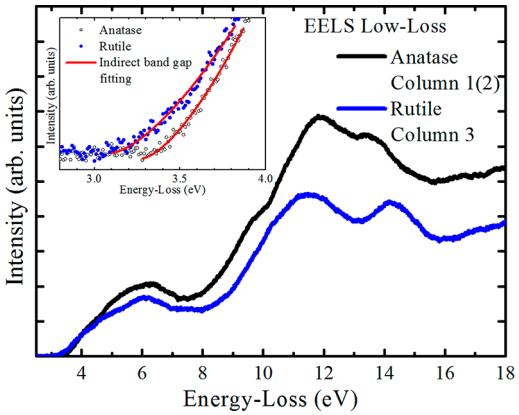

Figure 3. Low-loss EELS measurements of columns 1 and 3 according to the attribution made in Figure 1b. The inset shows a zoom in the 2.8−4.0 eV range, and the red lines are the Tauc fittings obtained for each column.

Therefore, from EELS results, we confirmed the presence of rutile and anatase phases in our TiO_2 films. Moreover, we note that the SEM image in Figure 1a and the TEM bright-field cross section image of Figure 1b combined with the EELS results show that the anatase phase is predominant over the surface areas and also in the film volume. Raman spectra were performed (see Figure S4), and there is a qualitative agreement between the Raman spectrum and the composition that can be deduced from TEM and SEM images.

The growth of rutile phase on top of *c*-sapphire is expected due to a lower lattice mismatch than the one formed in the anatase/*c*-sapphire interface.[26] However, in the Ti−O equilibrium phase diagram the stable phase below ∼600 °C is the anatase one.[10] For this temperature condition, Chang et al.[26] suggested that below a critical film thickness (d_c) the growth of rutile grains is favored due to the better lattice mismatch with *c*-sapphire and that above d_c anatase growth prevails. Another important factor determining the phase of the films is the energy distribution of the plasma particles hitting the substrate. As pointed by Mráz and Schneider,[20] processes involving higher energy distributions of the particles colliding with the film surface favor the formation of the rutile phase, while processes at lower powers and/or larger values of the pressure × distance parameter, proportional to the number of gas collisions and thermalization of the particles coming from the target, favor the anatase phase. On the present conditions, the pressure × distance is 23.3 Pa·mm, which is expected to favor the rutile growth.[20]

Considering these main factors of the growth, we can conclude that, in spite of the relatively low substrate temperature used, the films present a high rutile component due to the interface energy (film−substrate and anatase−rutile) and to the energetic collisions of plasma particles during growth. This complex relationship among the main growth components may explain the mixture of the anatase and rutile phases shown for the grown films. Considering these factors it is possible to understand why other groups, working on similar but not exactly the same deposition conditions, had reported different results.[27]

The orientation texture of the observed crystallites on both phases in the overall film is a relevant feature concerning the surface morphology and reactivity. In the following the texture is analyzed using pole figures of selected planes.

DOI: 10.1021/acsaem.8b02171
ACS Appl. Energy Mater. 2019, 2, 2579−2584

Figure 4a shows the anatase {101} pole figure. Intensity spots centered at χ equal to 41.0° and 68.2° are observed,

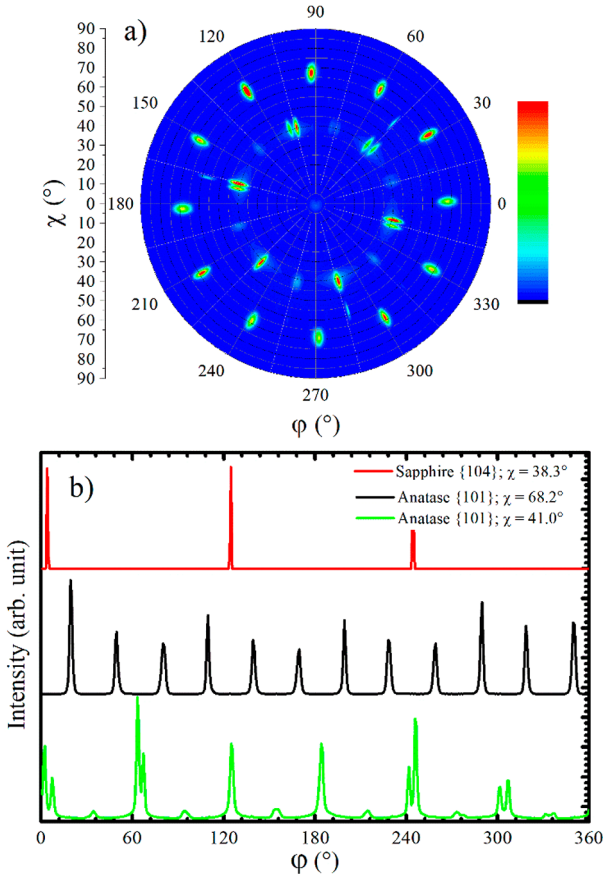

Figure 4. (a) Anatase {101} pole figure performed at 2θ = 25.224° for sample grown on *c*-sapphire. In the color scale bar red (blue) indicates high (low) counts. (b) Azimuthal scans for sapphire {104} at χ = 38.3° and for anatase {101} at χ = 68.2° and χ = 41.0°.

which are the angles of anatase {101} planes with anatase {112} and anatase {001} planes, respectively. It indicates the presence of anatase crystals with ⟨112⟩ and ⟨001⟩ out-of-plane orientations, which is consistent with the observation of anatase (112) and (004) peaks in the Bragg–Brentano measurement (see Figure S1).

Azimuthal scans for anatase grains growing in the ⟨001⟩ and ⟨112⟩ directions and sapphire ⟨0001⟩ are presented in Figure 4b. For anatase ⟨001⟩ 12 peaks spaced by 30° with respect to each other are observed. The presence of 12 peaks is due to the 4-fold and 3-fold symmetry of anatase {001} and sapphire {0001} planes, respectively. Anatase {112} planes also have 4-fold symmetry and consequently 12 peaks in the azimuthal curve. The double-peak structure and variation in the peak intensity are possibly related to lattice relaxation processes during anatase ⟨112⟩ growth. Similar double-peak structure has been previously observed for anatase films grown on lanthanum aluminate and associated with lattice relaxation.[28]

To analyze the texture of rutile grains, the rutile {110} pole figure was performed by setting 2θ = 27.434° (Figure 5a). It shows six sharp peaks centered at an angle χ = 45°, which exactly matches the angle between rutile {110} and {100} planes. Therefore, the ⟨100⟩ directions of rutile grains line up to the normal of both sapphire *c*-plane and substrate surface, allowing the {100} plane diffractions to be observed in Bragg–

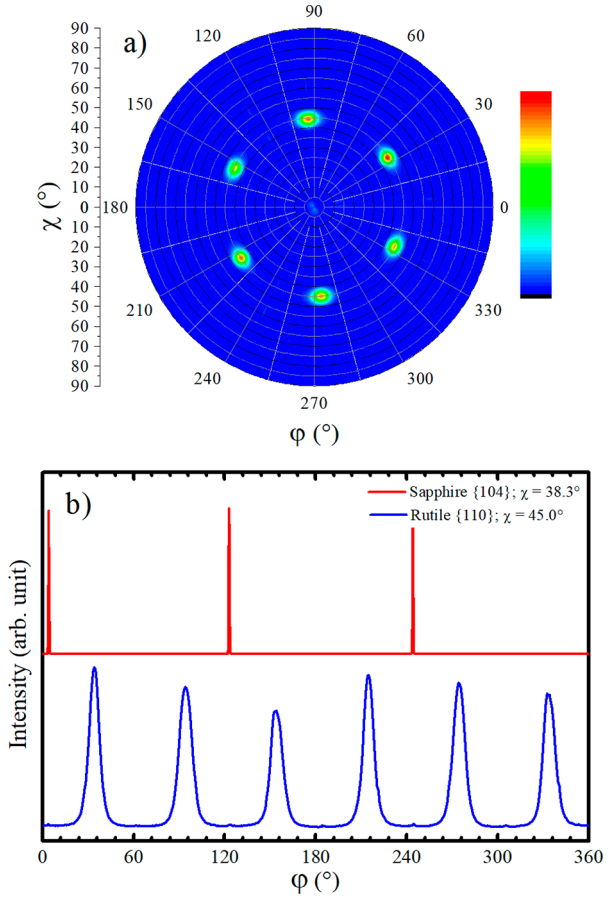

Figure 5. (a) Pole figure of rutile {110} (2θ = 27.434°) and (b) azimuthal scans for the TiO_2 film grown on *c*-sapphire substrate. In the color scale bar of (a), red (blue) indicates high (low) counts.

Brentano scans (Figure S1). The dependence of the film texture on the substrate nature was verified by growing a TiO_2 film on *a*-plane sapphire using the same deposition conditions employed for TiO_2 growth on *c*-plane sapphire. The rutile {110} pole figure (Figure S3) for the TiO_2 film grown on *a*-sapphire shows very different features if compared with Figure 5a, demonstrating distinct out-of-plane and in-plane orientations for TiO_2 films grown on *a*-sapphire and *c*-sapphire.

Azimuthal scans of TiO_2 film grown on *c*-sapphire for χ = 45.0° at 2θ = 27.434° and χ = 38.3° at 2θ = 35.167° are presented in Figure 5b. The first and second scans select rutile {110} and sapphire {104} planes, respectively. The expected presence of three peaks for sapphire is in accordance with the 3-fold symmetry of sapphire {0001} planes. For rutile six peaks spaced by 60° are observed and there is a 30° offset with respect to the sapphire ones. The quantity of six peaks is due to the 2-fold symmetry of rutile {100} plane and its three equivalent orientations on top of *c*-sapphire.[29]

According to SEM, TEM, and XRD results, the TiO_2 film deposited on *c*-sapphire presents a coherent growth, the anatase and rutile phases having in-plane and out-of-plane crystalline texture. Rocking curves (RCs) of rutile (200), anatase (004), and anatase (112) demonstrated that both phases present a low out-of-plane mosaicity. This is especially valid to rutile grains since rutile (200) RC has a full width at half maximum (fwhm) of only ∼0.1° (as shown in Figure S2). This value is very similar to the ones obtained for TiO_2 grown via atomic layer deposition,[30] chemical vapor deposition,[26,31]

DOI: 10.1021/acsaem.8b02171
ACS Appl. Energy Mater. 2019, 2, 2579–2584

and molecular beam epitaxy.[32] Therefore, the present growth conditions produce samples of high crystallinity, and the presence of amorphous material, in the grain interfaces, is difficult to detect, as seen by the tight fit between anatase and rutile crystals shown in Figure 1c. Both of these characteristics are favorable for transport and spatial charge separation of electron−hole pairs formed from light absorption.

Besides possessing desired crystalline and electronic properties for photocatalysis, the film also presents exposed anatase {001} facets, which are known to be the most reactive anatase facets.[4−9] In the films, the anatase grains with parallelepiped shape (see structure 1 in Figure 1a) have ⟨001⟩ out-of-plane orientation, and consequently the upper face of these grains is {001} facets. The growth of TiO_2 crystals with exposed {001} facets is generally thermodynamically unfavorable and grains with {101} facets are more favorable to be obtained.[11] However, the employed deposition conditions of the analyzed film allowed the growth of an expressive number of anatase grains with exposed {001} facets. The high reactivity of the {001} facets allied to the crystallinity, and favorable band alignment of the film is likely to promote high performance in photocatalytic reactions.

In spite of the fact that the electronic microscopy and Raman scattering results show the predominance of the anatase phase on the film bulk and indicate that the surface is dominated by the anatase phase, a direct and specific measurement of the contribution of each phase on the film surface could not be directly performed here. Concerning the XPS analysis, the difficulty is due to the fact that the differences in binding energy of photoelectrons in the Ti $2p_{3/2}$ are the order of 0.1 eV, while the fwhm of the peaks is about 1.3 eV.[18,33,34] These small peak shifts and wide line profiles result in a large superposition of the contributions related to anatase and rutile, making the deconvolution inaccurate. The Ti 2p peaks are shown in the Supporting Information (Figure S5), but because of the mentioned superposition, no reliable deconvolution procedure was possible.

In this way, besides maximizing the exposure of anatase {001} on the surfaces of films, it was possible to reach our goal in developing a technique with the potential to produce cost-effective films over large areas to favoring industrial applications of TiO_2 films to photocatalysis. Even though the sapphire (0001) substrates are still relatively expensive, as compared to borosilicate glass or commercial stainless steel, those are much cheaper than LAO (001) substrates, used many times in the growth of epitaxial TiO_2 with the desired (001) surface using MBE[17,35] and PLD.[36−38] Also, the natural capability of the reactive sputtering in producing homogeneous films over large areas provides remarkable advantage in terms of costs as compared to MBE production. Moreover, using the present set of parameters, we obtained rutile crystals in close contact with the anatase ones which is considered beneficial to the photocatalytic activity of the films.[12−17]

4. CONCLUSIONS

In summary, we demonstrated that the combination of substrate surface symmetry with the growth by reactive sputtering is found to produce peculiar arrangement in the growth of TiO_2 films. Rutile and anatase microcrystals grow coherently (articulately) onto sapphire substrates. In the arrangement the rutile phase presents highly ordered out of plane texture and three different in plane orientations, while the anatase presents two out of plane preferential axis (⟨100⟩ and ⟨112⟩). The more reactive anatase {001} facets are predominantly exposed on film surfaces. Because the sputtering technique allows the deposition over large areas, the process developed here could promote an efficiency improvement in photocatalytic applications of TiO_2.

■ ASSOCIATED CONTENT

Supporting Information

The Supporting Information is available free of charge on the ACS Publications website at DOI: 10.1021/acsaem.8b02171.

X-ray diffraction measurements, X-ray photoelectron spectroscopy, and Raman scattering (PDF)

■ AUTHOR INFORMATION

Corresponding Author

*(I.S.B.) E-mail iuri.brandt@pgfsc.ufsc.br.

ORCID

Iuri S. Brandt: 0000-0003-1144-9690

Notes

The authors declare no competing financial interest.

■ ACKNOWLEDGMENTS

The authors would like to thank Carlos Guilherme G. Azevedo for the assistance with sample preparation, Elvis Lopez Meza and Alexandre Mello for XPS measurements, and the International Iberian Nanotechnology Laboratory for making its electron microscopy facility available for the present work. We also would like to thank the Brazilian agencies CNPq, CAPES, FINEP, and FAPESP 2017/18916-7.

■ REFERENCES

(1) Linsebigler, A. L.; Lu, G.; Yates, J. T. Photocatalysis on TiO_2 Surfaces: Principles, Mechanisms, and Selected Results. *Chem. Rev.* **1995**, *95*, 735−758.

(2) Henderson, M. A. A Surface Science Perspective on TiO_2 Photocatalysis. *Surf. Sci. Rep.* **2011**, *66*, 185−297.

(3) Hashimoto, K.; Irie, H.; Fujishima, A. Photocatalysis: A Historical Overview and Future Prospects. *Jpn. J. Appl. Phys.* **2005**, *44*, 8269−8285.

(4) Yang, H. G.; Sun, C. H.; Qiao, S. Z.; Zou, J.; Liu, G.; Smith, S. C.; Cheng, H. M.; Lu, G. Q. Anatase TiO_2 Single Crystals with a Large Percentage of Reactive Facets. *Nature* **2008**, *453*, 638−641.

(5) Yang, H. G.; Liu, G.; Qiao, S. Z.; Sun, C. H.; Jin, Y. G.; Smith, S. C.; Zou, J.; Cheng, H. M.; Lu, G. Q. Solvothermal Synthesis and Photoreactivity of Anatase TiO_2 Nanosheets with Dominant {001} Facets. *J. Am. Chem. Soc.* **2009**, *131*, 4078−4083.

(6) Han, X.; Kuang, Q.; Jin, M.; Xie, Z.; Zheng, L. Synthesis of Titania Nanosheets with a High Percentage of Exposed (001) Facets and Related Photocatalytic Properties. *J. Am. Chem. Soc.* **2009**, *131*, 3152−3153.

(7) Zhang, D.; Li, G.; Yang, X.; Yu, J. C. A Micrometer-Size TiO_2 Single-Crystal Photocatalyst with Remarkable 80% Level of Reactive Facets. *Chem. Commun.* **2009**, No. 29, 4381−4383.

(8) Xiang, Q.; Lv, K.; Yu, J. Pivotal Role of Fluorine in Enhanced Photocatalytic Activity of Anatase TiO_2 Nanosheets with Dominant (001) Facets for the Photocatalytic Degradation of Acetone in Air. *Appl. Catal., B* **2010**, *96*, 557−564.

(9) Amano, F.; Prieto-Mahaney, O. O.; Terada, Y.; Yasumoto, T.; Shibayama, T.; Ohtani, B. Decahedral Single-Crystalline Particles of Anatase titanium(IV) Oxide with High Photocatalytic Activity. *Chem. Mater.* **2009**, *21*, 2601−2603.

(10) Hanaor, D. A. H.; Sorrell, C. C. Review of the Anatase to Rutile Phase Transformation. *J. Mater. Sci.* **2011**, *46* (4), 855−874.

DOI: 10.1021/acsaem.8b02171
ACS Appl. Energy Mater. 2019, 2, 2579−2584

(11) Lazzeri, M.; Vittadini, A.; Selloni, A. Structure and Energetics of Stoichiometric TiO_2 Anatase Surfaces. *Phys. Rev. B: Condens. Matter Mater. Phys.* **2001**, *63*, 1−9.
(12) Ohno, T.; Sarukawa, K.; Tokieda, K.; Matsumura, M. Morphology of a TiO_2 Photocatalyst (Degussa, P-25) Consisting of Anatase and Rutile Crystalline Phases. *J. Catal.* **2001**, *203*, 82−86.
(13) Li, W.; Liu, C.; Zhou, Y.; Bai, Y.; Feng, X.; Yang, Z.; Lu, L.; Lu, X.; Chan, K. Enhanced Photocatalytic Activity in Anatase/TiO_2(B) Core-Shell Nanofiber. *J. Phys. Chem. C* **2008**, *112*, 20539−20545.
(14) Yan, M.; Chen, F.; Zhang, J.; Anpo, M. Preparation of Controllable Crystalline Titania and Study on the Photocatalytic Properties. *J. Phys. Chem. B* **2005**, *109*, 8673−8678.
(15) Zhang, X.; Lin, Y.; He, D.; Zhang, J.; Fan, Z.; Xie, T. Interface Junction at Anatase/rutile in Mixed-Phase TiO_2: Formation and Photo-Generated Charge Carriers Properties. *Chem. Phys. Lett.* **2011**, *504*, 71−75.
(16) Hurum, D. C.; Agrios, A. G.; Gray, K. A.; Rajh, T.; Thurnauer, M. C. Explaining the Enhanced Photocatalytic Activity of Degussa P25 Mixed-Phase TiO_2 Using EPR. *J. Phys. Chem. B* **2003**, *107*, 4545−4549.
(17) Shao, R.; Wang, C.; McCready, D. E.; Droubay, T. C.; Chambers, S. A. Growth and Structure of MBE Grown TiO_2 Anatase Films with Rutile Nano-Crystallites. *Surf. Sci.* **2007**, *601*, 1582−1589.
(18) Scanlon, D. O.; Dunnill, C. W.; Buckeridge, J.; Shevlin, S. A.; Logsdail, A. J.; Woodley, S. M.; Catlow, C. R. A.; Powell, M. J.; Palgrave, R. G.; Parkin, I. P.; Watson, G. W.; Keal, T. W.; Sherwood, P.; Walsh, A.; Sokol, A. A. Band Alignment of Rutile and Anatase TiO_2. *Nat. Mater.* **2013**, *12*, 798−801.
(19) Mi, Y.; Weng, Y. Band Alignment and Controllable Electron Migration between Rutile and Anatase TiO_2. *Sci. Rep.* **2015**, *5*, 11482.
(20) Mráz, S.; Schneider, J. M. Structure Evolution of Magnetron Sputtered TiO_2 Thin Films Structure Evolution of Magnetron Sputtered TiO_2 Thin Films. *J. Appl. Phys.* **2011**, *109*, 023512.
(21) Gloter, A.; Ewels, C.; Umek, P.; Arcon, D.; Colliex, C. Electronic Structure of Titania-Based Nanotubes Investigated by EELS Spectroscopy. *Phys. Rev. B: Condens. Matter Mater. Phys.* **2009**, *80*, 1−6.
(22) Launay, M.; Boucher, F.; Moreau, P. Evidence of a Rutile-Phase Characteristic Peak in Low-Energy Loss Spectra. *Phys. Rev. B: Condens. Matter Mater. Phys.* **2004**, *69*, 35101.
(23) Rafferty, B.; Brown, L. Direct and Indirect Transitions in the Region of the Band Gap Using Electron-Energy-Loss Spectroscopy. *Phys. Rev. B: Condens. Matter Mater. Phys.* **1998**, *58*, 10326−10337.
(24) Tang, H.; Lévy, F.; Berger, H.; Schmid, P. E. Urback Tail of Anatase TiO_2. *Phys. Rev. B: Condens. Matter Mater. Phys.* **1995**, *52*, 7771−7774.
(25) Forro, L.; Chauvet, O.; Emin, D.; Zuppiroli, L.; Berger, H.; Lévy, F. High Mobility N-Type Charge Carriers in Large Single Crystals of Anatase (TiO_2). *J. Appl. Phys.* **1994**, *75*, 633−635.
(26) Chang, H. L. M.; Zhang, T. J.; Zhang, H.; Guo, J.; Kim, H. K.; Lam, D. J. Epitaxy, Microstructure, and Processing-Structure Relationships of TiO_2 Thin Films Grown on Sapphire (0001) by MOCVD. *J. Mater. Res.* **1993**, *8*, 2634−2643.
(27) Lee, G.-H.; Kim, M.-S. Crystal Structure of TiO_2 Thin Films Grown on Sapphire Substrates by RF Sputtering as a Function of Temperature. *Electron. Mater. Lett.* **2010**, *6*, 77−80.
(28) Brandt, I. S.; Plá Cid, C. C.; Azevedo, C. G. G.; Pereira, A. L. J.; Benetti, L. C.; Ferlauto, A. S.; Dias da Silva, J. H.; Pasa, A. A. Influence of Substrate on the Structure of Predominantly Anatase TiO_2 Films Grown by Reactive Sputtering. *RSC Adv.* **2018**, *8*, 7062−7071.
(29) Bayati, M. R.; Joshi, S.; Narayan, R. J.; Narayan, J. Low-Temperature Processing and Control of Structure and Properties of TiO_2/c-Sapphire Epitaxial Heterostructures. *J. Mater. Res.* **2013**, *28*, 1669−1679.
(30) Tarre, A.; Möldre, K.; Niilisk, A.; Mändar, H.; Aarik, J.; Rosental, A. Atomic Layer Deposition of Epitaxial TiO_2 II on c-Sapphire. *J. Vac. Sci. Technol., A* **2013**, *31*, No. 01A118.
(31) Schuisky, M.; Hårsta, A.; Aidla, A.; Kukli, K.; Kiisler, A.; Aarik, J. Atomic Layer Chemical Vapor Deposition of TiO_2 Low Temperature Epitaxy of Rutile and Anatase. *J. Electrochem. Soc.* **2000**, *147*, 3319−3325.
(32) Engel-Herbert, R.; Jalan, B.; Cagnon, J.; Stemmer, S. Microstructure of Epitaxial Rutile TiO_2 Films Grown by Molecular Beam Epitaxy on R-Plane Al_2O_3. *J. Cryst. Growth* **2009**, *312*, 149−153.
(33) Herman, G. S.; Gao, Y.; Tran, T. T.; Osterwalder, J. X-Ray Photoelectron Di Raction Study of an Anatase Thin Lm: TiO_2(001). *Surf. Sci.* **2000**, *447*, 201−211.
(34) Das, C.; Richter, M.; Tallarida, M.; Schmeisser, D. Electronic Properties of Atomic Layer Deposition Films, Anatase and Rutile TiO_2 Studied by Resonant Photoemission Spectroscopy. *J. Phys. D: Appl. Phys.* **2016**, *49*, 275304.
(35) Chambers, S. A.; Wang, C. M.; Thevuthasan, S.; Droubay, T.; Mccready, D. E.; Lea, A. S.; Shutthanandan, V.; Windisch, C. F., Jr. Epitaxial Growth and Properties of MBE-Grown Ferromagnetic Co-Doped TiO_2 Anatase Films on SrTiO3 (001) and LaAlO3 (001). *Thin Solid Films* **2002**, *418*, 197−210.
(36) Yamamoto, S.; Sumita, T.; Miyashita, A.; Naramoto, H. Preparation of Epitaxial TiO_2 Films by Pulsed Laser Deposition Technique. *Thin Solid Films* **2001**, *401*, 88−93.
(37) Krupski, K.; Sanchez, A. M.; Krupski, A.; McConville, C. F. Applied Surface Science Optimisation of Anatase TiO_2 Thin Film Growth on $LaAlO_3$ (001) Using Pulsed Laser Deposition. *Appl. Surf. Sci.* **2016**, *388*, 684−690.
(38) Benetti, D.; Nouar, R.; Nechache, R.; Pepin, H.; Sarkissian, A.; Rosei, F.; Macleod, J. M. Combined Magnetron Sputtering and Pulsed Laser Deposition of TiO_2 and BFCO Thin Films. *Sci. Rep.* **2017**, *7*, 1−9.

DOI: 10.1021/acsaem.8b02171
ACS Appl. Energy Mater. 2019, 2, 2579−2584